Volume 1 | Number 1 | Jan 2013 | Pages 1–100

Journal of
Materials Chemistry A

Materials for energy and sustainability
www.rsc.org/materialsA

Li+

ROYAL SOCIETY
OF CHEMISTRY

ROYAL SOCIETY
OF CHEMISTRY

www.rsc.org/materialsA

1 **Metal organic framework derived magnetic porous carbon composites supported**

2 **gold and palladium nanoparticles as highly efficient and recyclable catalysts for**

3 **reduction of 4-nitrophenol and hydrodechlorination of 4-chlorophenol**

4

5 Zhengping Dong*, Xuanduong Le, Yansheng Liu, Chunxu Dong, Jiantai Ma*

6 *College of Chemistry and Chemical Engineering, Gansu Provincial Engineering Laboratory for*

7 *Chemical Catalysis, Lanzhou University, Lanzhou 730000, PR China*

8

9 *Corresponding author. Tel.: +86 0931 8912577; fax: +86 0931 8912582.

10 *E-mail address*: dongzhp@lzu.edu.cn (Zhengping Dong), majiantai@lzu.edu.cn (Jiantai Ma)

11

12 **Abstract**

13 The development of low cost noble metal nanocatalysts with high activity and

14 selectivity, high catalytic performance, convenient separation, and reusability is a

15 significant challenge. Herein, the magnetic porous carbon (MPC) composite,

16 synthesized from metal organic framework (MOF) was used as catalyst support to

17 fabricate gold (Au) and palladium (Pd) nanoparticles (NPs) based nanocatalysts. The

18 MPC not only provided a large surface area and mesopores on which the active

19 centers (Au and Pd NPs) were finely dispersed, but also exhibited superparamagnetic

20 behaviour that enabled the magnetic separation and convenient recovery of the

21 nanocatalysts from the reaction mixture. Thus, the nanocatalysts were repeatedly used

22 without loss of catalytic efficiency. Both the Au/MPC and Pd/MPC nanocatalysts

23 showed excellent catalytic activity for the reduction of 4-nitrophenol. Moreover, the

24 Pd/MPC nanocatalyst exhibited higher efficiency toward hydrodechlorination of

25 4-chlorophenol compared to the other reported catalysts. This study indicated that the

26 noble metal NPs (NMNPs) supported on MOF-derived MPC materials could act as

27 promising catalysts exhibiting potential applications in numerous NMNPs based

28 catalytic reactions.

29

1   Introduction

2   Recently, noble metal nanoparticles (NMNPs) based heterogeneous catalysts have

3   attracted significant attention in catalysis science due to their high efficiency in

4   numerous liquid-phase catalytic processes. In particular, gold (Au) and palladium (Pd)

5   nanoparticles (NPs) based catalysts have been extensively studied in many organic

6   catalytic reactions, including C–C cross-coupling, hydrogenation, and methanol

7   oxidation.[1-8] However, the surface energy of NMNPs increases with decrease in the

8   particle size; therefore, NMNPs with smaller particle size have the tendency of

9   inter-particle aggregation, which eventually reduces the catalytic efficiency of the

10 catalysts.[9, 10] Thus, stability of the NMNPs is another crucial issue for their further

11 application. The emergence of new nanomaterials like mesoporous silica,[11]

12 graphene,[12] MoS_x,[13] and metal organic frameworks (MOFs)[14] are promising supports

13 to fabricate composite catalysts to solve this problem. Therefore, carbonaceous

14 materials, such as active carbons, carbon nanotubes, and graphene have been

15 conventionally used as efficient support materials for preparing heterogeneous

16 NMNPs catalysts, due to their excellent mechanical strength, chemical stability, and

17 large surface area.[15-19] However, the micropores of the active carbons are blocked

18 easily by NMNPs, which further hinders the diffusion of reactants and products into

19 their pore texture. Moreover, NMNPs which are physically attached to carbon

20 nanotubes and graphene always undergo easy leaching during the catalytic process,

21 and leaching is a detrimental factor that induces significant loss of catalytic activity.

22 Only functionalized with N- and O-containing functional groups, the NMNPs on these

23 carbon materials could not be easily leaching and subsequently enhance the catalytic

24 activity.[12] Further, high cost and limited resources of noble metals also hinder their

25 practical application. Therefore, to overcome the above mentioned issues, design of

26 heterogeneous NMNPs catalysts that preserve high metal dispersion and stability

27 during the catalytic reactions and easily separate from the reaction mixture, is of

28 significant importance.[20] In recent years, utilization of MOFs as templates or

29 precursor materials for the production of porous carbon materials has been effectively

1   demonstrated by taking advantage of the fact that MOFs are porous materials and

2   possess a significant amount of carbon source.[21-24] Recently reported magnetic porous

3   carbon (MPC) composites, derived from MOF, exhibiting mesoporous structure,

4   magnetic separability, and recyclability act as excellent candidates for the NMNPs

5   catalysts support.[23, 24] However, related work has rarely been reported.

6   Green chemistry has attracted considerable attention to overcome the problem

7   pertaining to the environmental pollution being encountered by the global population.

8   4-nitrophenol (4-NP) and 4-chlorophenol (4-CP) are useful industrial chemicals to

9   synthesize numerous chemical products. However, as industrial pollutants they exhibit

10 high toxicity and poor biological degradability.[25-28] In this aspect, disposal of 4-NP

11 and 4-CP is an area of intensive research. Among most of the reported methods,

12 reduction of 4-NP and hydrodechlorination (HDC) of 4-CP are considered to be the

13 most effective methods because the reduction product 4-aminophenol (4-AP) is an

14 extremely useful organic compound employed in various applications,[29] and the HDC

15 product (phenol) can also be subsequently recycled. Therefore, design of catalysts

16 with high catalytic activity and potential practical application for reduction of 4-NP

17 and HDC of 4-CP is of significant importance. A rapid, efficient, and green approach

18 to the fabrication of efficient catalysts for reduction of 4-NP and HDC of 4-CP is

19 highly desirable.

20 Based on the abovementioned perspective, in this study, two NMNPs (Au and Pd)

21 were successfully immobilized on the magnetic mesoporous carbon matrices derived

22 from MOFs to fabricate Au/MPC and Pd/MPC nanocatalysts. In both the synthesized

23 nanocatalysts, the MPC provided a large surface area and mesopores on which the

24 active centers (Au and Pd NPs) were finely dispersed. The nanocatalysts could be

25 easily recovered from the reaction mixture by a magnet because of the magnetic NPs

26 encapsulated in the porous carbon, and conveniently reused. Both the Au/MPC and

27 Pd/MPC nanocatalysts exhibited excellent catalytic activity toward the reduction of

28 4-NP than most of the other reported catalysts. Moreover, the Pd/MPC nanocatalyst

29 showed high efficiency toward HDC of chlorophenols. Thus, this study involving

30 Au/MPC and Pd/MPC nanocatalysts provided a useful platform for exploring

1 environmentally friendly NMNPs based catalysts with superior activity, convenient

2 recovery, and reusability.

3 **Experimental**

4 *Materials*

5 HPLC grade ethyl acetate ($CH_3COOC_2H_5$), chloroauric acid ($HAuCl_4 \cdot 4H_2O$), and

6 palladium chloride ($PdCl_2$) were purchased from Sigma Aldrich and used as received.

7 Fumaric acid, $Fe(NO_3)_3 \cdot 9H_2O$, *N,N*-dimethylformamide (DMF), Sodium borohydride

8 ($NaBH_4$), 4-NP, and CPs were purchased from Shanghai Chemical Reagent Co., Ltd.

9 All other chemicals were of reagent grade purchased from Tianjin Guangfu Chemical

10 Company and used as supplied.

11 *Synthesis of MPC composites*

12 MPC composites were synthesized according to a similar route reported by

13 Moonhyun Oh.[24] The MOF composite, namely, iron(III) dicarboxylate MOFs of the

14 MIL-88 structure type (Fe-MIL-88A), were first prepared according to the reported

15 solvothermal method using $Fe(NO_3)_3$ and fumaric acid.[30] Fumaric acid (1.68 g, 14.4

16 mmol) and $Fe(NO_3)_3 \cdot 9H_2O$ (6.4 g, 16 mmol) were dissolved in DMF (300 mL). The

17 resulting mixture was then heated to 110 °C and allowed to stand for 1 h. The

18 resulting Fe-MIL-88A was obtained by successively washing with DMF and methanol

19 via centrifugation redispersion cycles. Subsequently, the as-prepared Fe-MIL-88A (2

20 g) was placed in a tube furnace and calcined up to 700 °C under a nitrogen gas flow at

21 a heating rate of 5 °C min^{-1} and held at 700 °C for 1 h. The resulting MPC composites

22 were cooled to room temperature.

23 *Preparation of Au/MPC nanocatalyst*

24 The Au/MPC nanocatalyst was prepared by the method similar to the preparation of

25 Au/C catalyst.[31, 32] Briefly, MPC (500 mg) was dispersed in water (H_2O, 20 mL) by

26 ultrasonication. This was followed by the addition of $HAuCl_4$ (10 mL, C_{Au} = 2.5 mg

27 mL^{-1}) to the aqueous solution by ultrasonic agitation for 30 min. Subsequently, the

mixture was adjusted to alkalescence using ammonia and freshly prepared $NaBH_4$

solution was rapidly added to the mixture under vigorous stirring, followed by further

stirring for 12 h and ageing for 24 h. The contents were filtered to afford Au/MPC

nanocatalyst. The as-prepared nanocatalyst was washed adequately with distilled

water and dried in an oven at 60 °C for 5 h.

Fabrication of Pd/MPC nanocatalyst

The Pd/MPC nanocatalyst was prepared by the following method:[33] First, $PdCl_2$ was

dissolved in the solution of KCl to form $[PdCl_4]^{2-}$ complex. Second, MPC (800 mg)

was dispersed in H_2O (20 mL), and the as-prepared K_2PdCl_4 solution (45 mL, C_{Pd} = 1

mg mL^{-1}) was added to the dispersion. Third, the reaction mixture was heated to

95 °C and five-fold excess amount of formaldehyde solution (28 wt%) was added

dropwise. Subsequently, the mixture was allowed to stir mildly for 1 h at 95 °C.

Finally, the Pd/MPC nanocatalyst was separated by filtration, washed with KCl

solution (0.5 wt%), and dried over night in an oven at room temperature.

Characterization

The morphology of the samples was characterized by transmission electron

microscopy (TEM) performed on a Tecnai G^2 F^{30} instrument operated at an

accelerating voltage of 200 kV. The samples were prepared by dispersing the

composites and nanocatalysts in C_2H_5OH deposited on a Cu-based TEM grid. Powder

X-ray diffraction (PXRD) measurements were performed on a Rigaku D/max-2400

diffractometer using Cu-Kα radiation as the X-ray source in the 2θ range of 20–85°.

The electronic states of the surface of the samples were analyzed by X-ray

photoelectron spectroscopy (XPS, Perkin-Elmer PHI-5702). The values of binding

energy were calibrated by using C1s = 284.6 eV as a reference. N_2 adsorption–

desorption isotherms were recorded at 77 K in a micromeritics ASAP 2010 (USA).

Specific surface areas (SBET) and average pore diameters (DP) were calculated using

the Brunauer–Emmett–Teller (BET) and Barrett–Joyner–Halenda (BJH) models,

respectively. Magnetic measurements on MPC composites, Au/MPC, and Pd/MPC

1 nanocatalysts were investigated by a quantum design vibrating sample magnetometer

2 (VSM) at room temperature in an applied magnetic field sweeping from −15 to 15

3 kOe. The Au and Pd content of the prepared nanocatalysts were obtained by the

4 inductively coupled plasma atomic emission spectroscopy (ICP–AES). Ultraviolet–

5 Visible (UV–Vis) spectrophotometer (Varian UV-Cary100) was utilized to obtain the

6 absorption spectra. The conversions of the HDC reactions were estimated by gas

7 chromatography–mass spectrometry (GC–MS, Shimadzu QP2010S).

8 *General procedure for the reduction of 4-NP*

9 First, 4-NP aqueous solution (0.01M, 30 μL) was mixed with H_2O (2.5 mL), then

10 freshly prepared aqueous $NaBH_4$ solution (0.5 M, 0.15 mL) was added, which

11 resulted in the formation of a deep yellow solution. Then, Au/MPC nanocatalyst (0.3

12 mL, 1 mg mL^{-1}) was added to the yellow solution and the reaction was continued

13 until the solution became colorless. For the reduction reaction catalyzed by Pd/MPC

14 nanocatalyst, the amounts of reactants used were 30 μL of 4-NP solution (0.01M), 2.8

15 mL of H_2O, 0.15 mL of $NaBH_4$ solution (0.5M), and 30 μL of Pd/MPC nanocatalyst

16 (concentration 1 mg mL^{-1}). The progress of the reduction process was monitored by

17 measuring the UV–Vis absorption spectra. In order to investigate the reusability of the

18 nanocatalysts, a magnet was used to recover the nanocatalysts for the next catalytic

19 run.

20 *General procedure for the HDC of 4-CP*

21 The experiments involving HDC of 4-CP were performed in a 50 mL two-necked

22 flask. The H_2 flow rate was 30 mL min^{-1} and a stirring speed of 600 rpm were set. In

23 general, catalyst (10 mL, 1 mg mL^{-1}), sodium hydroxide (NaOH) solution (10 mL,

24 0.05 M), and chlorophenol (10 mL, 0.05 M) were mixed in a 50 mL two-necked flask,

25 followed by bubbling H_2 into the reaction mixture and the reaction was timed

26 immediately. The sample was collected with a glass syringe at an interval of 10 min,

27 and then filtered through a 0.45 μm membrane filter. The filtrate was extracted by

28 $CH_3COOC_2H_5$, then the reaction conversion of the HDC reaction was estimated by

1 GC–MS. To evaluate the reusability of the Pd/MPC nanocatalyst in the HDC reaction,

2 the nanocatalyst was recovered using a magnet, washed with water, and dried in

3 vacuo at room temperature for the subsequent catalytic run. Moreover, the catalytic

4 procedure was repeated six times.

5 **Results and discussion**

6 The MPC nanorods were derived from the Fe-MIL-88A MOFs by a pyrolysis method.

7 In this study, mesoporous MPC composites consisting of pores with diameters of

8 about 10.9 nm, and surface area of about 138.74 $m^2\ g^{-1}$, exhibited excellent magnetic

9 property. Therefore, MPC was employed to fabricate highly efficient catalysts

10 (Au/MPC and Pd/MPC) exhibiting high catalytic activities and performance, and

11 convenient magnetic recovery.

12 *Characterization of the catalysts*

13

14
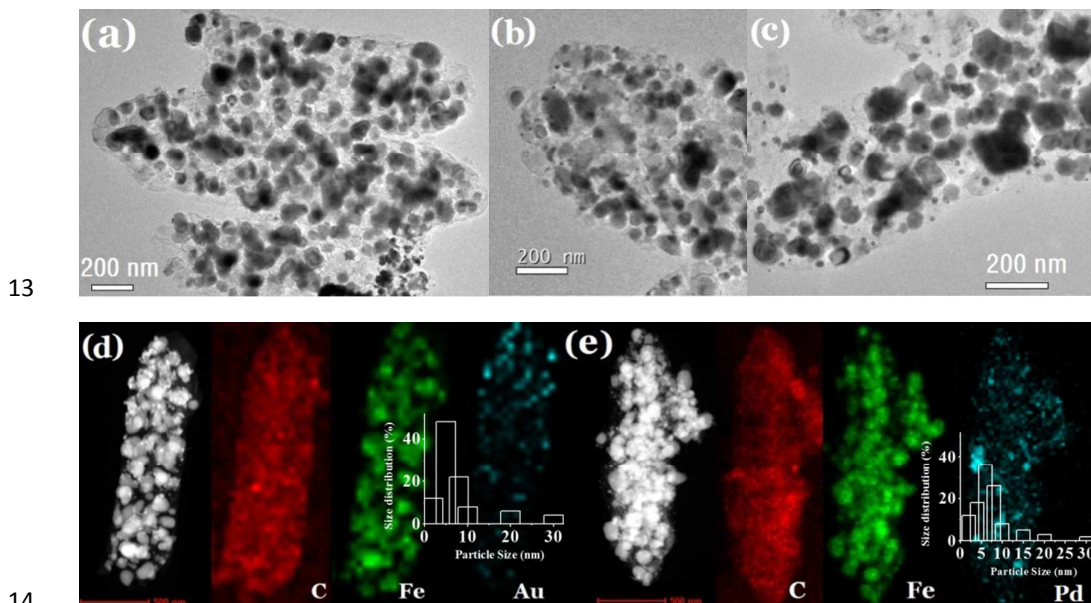
15 **Fig. 1.** TEM of (a) MPC, (b) Au/MPC and (c) Pd/MPC; (d) HAADF-STEM image of Au/MPC, C mapping image

16 (C-K), Fe mapping image (Fe-L), and Au mapping image (Au-L); (e) HAADF-STEM image of Pd/MPC, C

17 mapping image (C-K), Fe mapping image (Fe-L), and Pd mapping image (Pd-K).

18

19 The morphology and particle size of the MPC are displayed in Fig. 1a, which clearly

20 shows that MPC consists of magnetic iron oxide wrapped in the carbon (C)

21 framework. Moreover, the Figure exhibits that MPC has a diameter and length of

1   about 400 and 1,000 nm, respectively. The nanocatalysts Au/MPC and Pd/MPC were

2   prepared by impregnation–reduction method. Fig. 1b and 1c present the morphologies

3   of the Au/MPC and Pd/MPC nanocatalysts, respectively. Compared to Fig. 1a, the

4   TEM images exhibit tiny black dots without aggregation for both Au NPs (Fig. 1b)

5   and Pd NPs (Fig. 1c). Fig. 1d and 1e show high angle annular dark field–scanning

6   transmission electron microscopy (HAADF-STEM) images displaying a more

7   detailed elemental distribution of the nanocatalysts. The Figures clearly demonstrate

8   that the MPC support is mainly composed of C and Fe elements. As the catalytic

9   activity center, Au NPs (Fig. 1d) and Pd NPs (Fig. 1e) are dispersed in the MPC,

10   indicating the immobilization of Au NPs and Pd NPs in the pores of the mesoporous

11   MPC. From the HAADF-STEM image and the Au mapping image (Au-L), it can be

12   seen that the particle size of the Au NPs was mainly located in 5-8 nm. The particle

13   size of Pd NPs measured from Pd/MPC was about 5 nm.

14

15
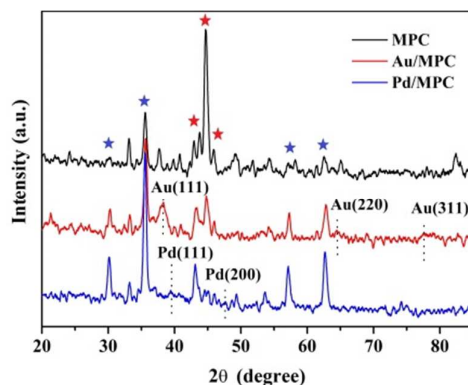
16   **Fig. 2.** PXRD patterns of MPC, Au/MPC and Pd/MPC (★ γ-Fe$_2$O$_3$ (JCPDS No. 39-1346), ★ Fe$_3$C (JCPDS No.

17   35-0772)).

18

19   PXRD analysis provided evidence for the composition of the as-synthesized samples.

20   Fig. 2 shows the PXRD patterns of MPC, revealing that γ-Fe$_2$O$_3$ and iron carbide

21   (Fe$_3$C) are the major products of the pyrolysis of Fe-MIL-88A at 700 °C. In fact, both

22   γ-Fe$_2$O$_3$ and magnetite (Fe$_3$O$_4$) have almost similar PXRD patterns; therefore, they

23   could not be easily distinguished by using only PXRD data. The formation of γ-Fe$_2$O$_3$

24   rather than Fe$_3$O$_4$ is confirmed from the XPS spectrum (Fig. 3), the characteristic

25   satellite peak for γ-Fe$_2$O$_3$ was observed at 719.9 eV.[24] The PXRD patterns of Au/MPC

1   and Pd/MPC (Fig. 2) also show the characteristic peaks of γ-Fe_2O_3 and Fe_3C.

2   However, compared to MPC, the PXRD patterns of Au/MPC show three

3   characteristic peaks located at 2θ = 38.4, 64.9, and 77.8° corresponding to the (111),

4   (220), and (311) lattice planes of Au (JCPDS, No. 4-0784), respectively. The PXRD

5   patterns of Pd/MPC also exhibit characteristic Pd NPs diffraction peaks (2θ = 39.8

6   and 47.5°) corresponding to (111) and (200) reflections, respectively. The above

7   mentioned PXRD results indicated that the Au and Pd NPs were successfully

8   immobilized in the pores of the mesoporous MPC support.
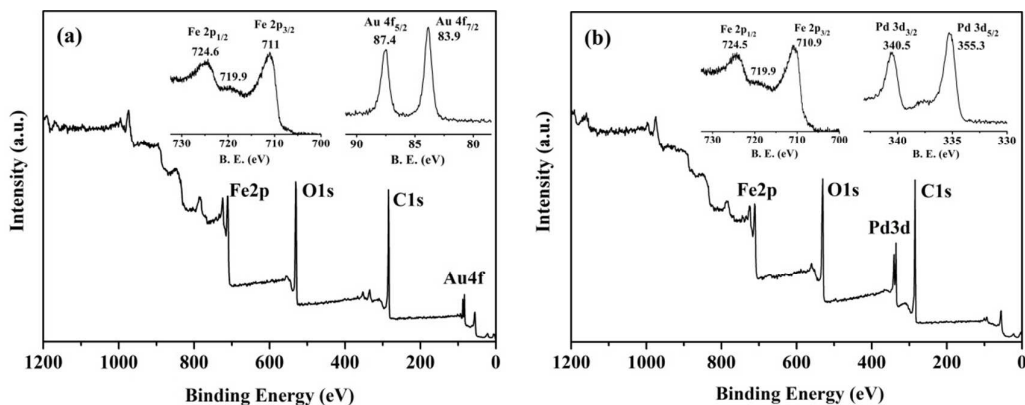
9
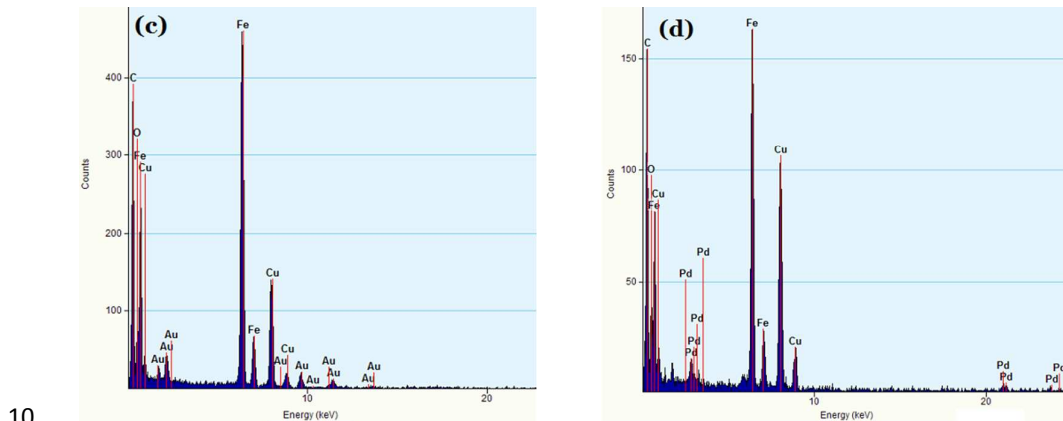
10

11   **Fig. 3.** XPS wide-scan spectra of (a) Au/MPC and (b) Pd/MPC nanocatalysts. EDS spectra of (c) Au/MPC and (d)

12   Pd/MPC nanocatalysts.

13

14   XPS was performed to investigate the chemical state of the surface of obtained

15   Au/MPC and Pd/MPC nanocatalysts (Fig. 3). Both the Fig. 3a and b show the broad

16   peaks assigned to Fe $2p_{1/2}$ and Fe $2p_{3/2}$, respectively. Moreover, characteristic peak for

17   γ-Fe_2O_3 at 719.9 eV is also observed. Fig. 3a shows the XPS spectrum of Au/MPC

18   nanocatalyst displaying two obvious Au 4f peaks, indicative of metallic Au at binding

1   energies of 83.9 and 87.4 eV, in Au $4f_{7/2}$ and Au $4f_{5/2}$ levels, respectively. Moreover,

2   for the Pd/MPC nanocatalyst (Fig. 3b), the characteristic peaks of metallic Pd NPs are

3   also clearly observed, the peaks at 335.3 and 340.5 eV are assigned to Pd $3d_{5/2}$ and Pd

4   $3d_{3/2}$, respectively. The energy dispersive spectrscopic (EDS) analysis was utilized to

5   determine the chemical composition of Au/MPC and Pd/MPC (Fig. 3c and d). Fig. 3c

6   exhibits the peaks corresponding to Fe, Au, C, and O revealing the compositions of

7   Au/MPC. The peaks corresponding to Fe, Pd, C, and O are presented in Fig. 3d,

8   indicating the compositions of Pd/MPC.

9   **Table 1.** The physical property parameters of MPC, Au/MPC and Pd/MPC.

Entry	Samples	Surface area (m^2/g)	Pore size (nm)	Au loading (wt%)	Pd loading (wt%)
1	MPC	138.74	10.9		
2	Au/MPC	118.06	8.5	3.93%	
3	Pd/MPC	101.9	8.9		5.11%

10
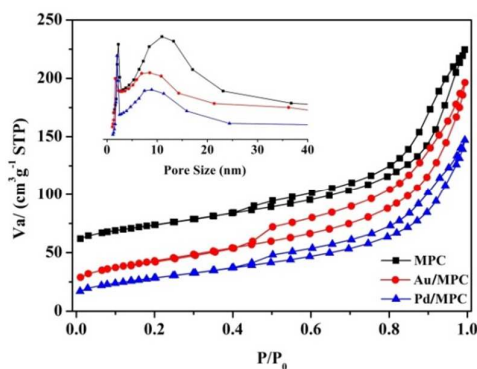
11   **Fig. 4.** N_2 sorption isotherms of MPC, Au/MPC and Pd/MPC (***Inset*** is the pore size distributions of MPC,
12   Au/MPC and Pd/MPC).

13

14   The mesoporosity of the as-synthesized materials was determined by nitrogen

15   physisorption measurements. The nitrogen adsorption–desorption isotherms of MPC,

16   Au/MPC and Pd/MPC are type-IV with a distinct hysteresis loop (Fig. 4). The main

17   pore size distribution of MPC, Au/MPC, and Pd/MPC is in the range from 5–20 nm

18   (Fig. 4 ***inset***). Both the results indicated that the MPC support, the Au/MPC and

19   Pd/MPC nanocatalysts had the mesoporous architecture. The physical property

20   parameters of MPC, Au/MPC, and Pd/MPC are listed in Table 1. The surface area and

21   pore size for MPC are 138.74 m^2 g^{-1} and 10.9 nm, respectively. When loaded with Au

22   or Pd NPs, the surface area and pore size of the samples reduced to 118.06 m^2 g^{-1} and

10

1   8.5 nm, respectively for Au/MPC, and 101.9 m^2 g^{-1} and 8.9 nm, respectively for

2   Pd/MPC. The values of weight percentage of Au or Pd loading obtained from ICP–

3   AES measurement are also listed in Table 1. There are about 3.93 wt% of Au NPs and

4   5.11 wt% of Pd NPs in Au/MPC and Pd/MPC nanocatalysts, respectively.

5   The superparamagnetic behaviour of the magnetic NPs is demonstrated by VSM

6   curves (Fig. 5). The magnetic saturation value for MPC composite was 76.5 emu g^{-1}.

7   When loaded with Au or Pd NPs, the magnetic saturation values reduced to 48.5 and

8   51.3 emu g^{-1}, respectively for Au/MPC and Pd/MPC nanocatalysts. Therefore, the

9   Au/MPC and Pd/MPC nanocatalysts could be efficiently separated from the reaction

10 solution by an external magnetic force, and could be reused and recycled (Fig. 5

11 *inset*).[34]
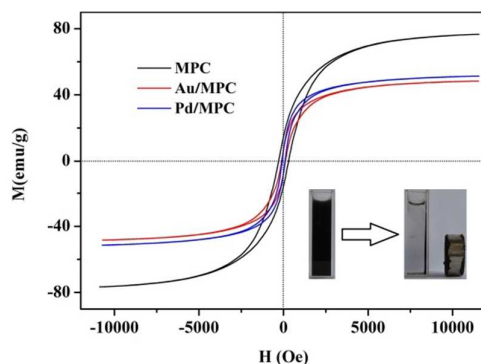
12

13   **Fig. 5.** Room temperature magnetization curves of MPC, Au/MPC and Pd/MPC.

14 ***Reduction of 4-NP***
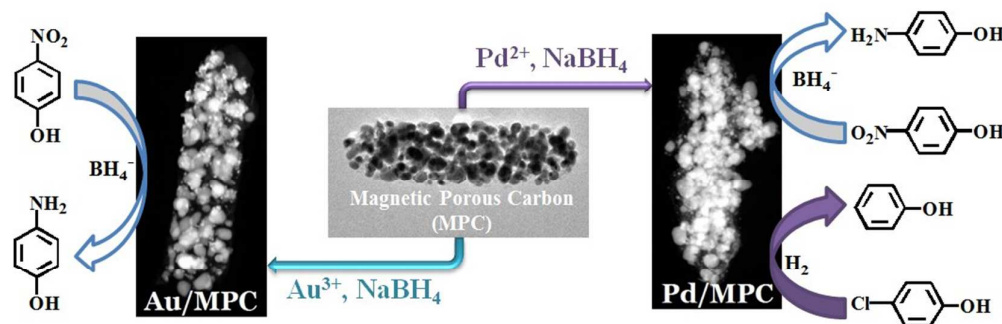
15

16   **Scheme 1.** MPC utilized as catalysts support to fabricate Au and Pd NPs based nanocatalysts.

17

18 Notably, metallic Au and Pd NPs are excellent catalysts with high activity and

1   selectivity.[35-39] Thus, Au and Pd NPs immobilized on MPC support could serve as a

2   practical recyclable heterogeneous catalyst (Scheme 1).

3   The catalytic performance of the as-prepared Au/MPC and Pd/MPC nanocatalysts was

4   initially evaluated by the reduction of 4-NP to 4-AP using excess of $NaBH_4$ under

5   ambient conditions. Aqueous solution of 4-NP is pale yellow and exhibits

6   a characteristic absorption peak centered around 317 nm (Fig. 6a). However, on

7   addition of $NaBH_4$, the color of the solution changes to yellow (Fig. S1a) indicating

8   the formation of 4-nitrophenolate ions due to the alkalinity of the solution.[40, 41] A new

9   absorption band appears at 400 nm (Fig. 6a) and the initial absorption band at 317 nm

10   vanishes completely. Interestingly, the reduction of the nitro-group does not proceed

11   in the absence of catalysts because the kinetic barrier between the mutually repelling

12   negative ions, 4-NP and BH_4^-, is extremely high.[36] Moreover, the reaction does not

13   proceed even for 5 h when catalyzed by MPC alone (Fig. S1b). In contrast, addition of

14   appropriate amount of catalyst (0.3 mg Au/MPC or 0.03 mg Pd/MPC) into the

15   solution resulted in decolorization of the 4-nitrophenolate solution, and

16   simultaneously the peak intensity at 400 nm successively decreased with the

17   appearance of the new adsorption peak at 300 nm (Fig. 6b and 6c). The above

18   phenomenons indicated that the catalyst support MPC had no catalytic activity in the

19   reduction of 4-NP. When MPC was functionalized with Au or Pd NPs, high catalytic

20   activity was then endowed to reduce 4-NP to 4-AP. The catalytic mechanism of the

21   reduction reaction was described as follows: adsorption of both the donor BH_4^- ions

22   and the acceptor 4-NP molecules onto the catalytic centers led to the electron transfer

23   from BH_4^- to 4-NP which resulted in the reduction of 4-NP.[36, 42] The UV–Vis spectra

24   showed an isosbestic point (313 nm), illustrating that the catalytic reduction of 4-NP

25   resulted in the formation of only 4-AP; thus excluding the formation of any

26   byproduct.[43]
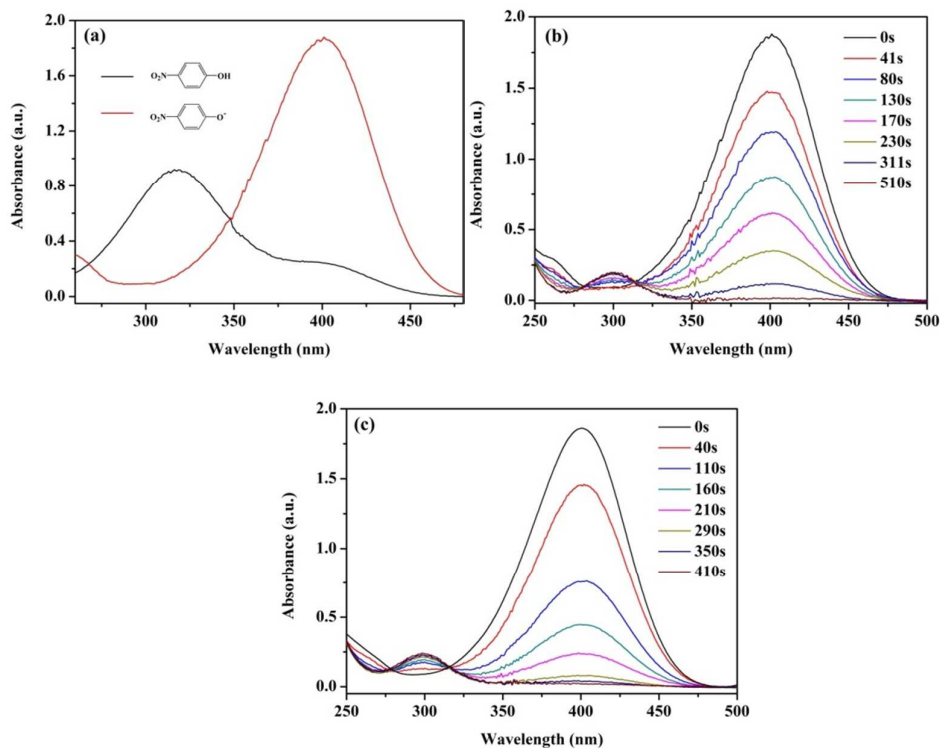
Fig. 6. UV-Vis spectra of 4-NP before and after adding $NaBH_4$ solution (a), the successive reduction of 4-NP to 4-AP over Au/MPC nanocatalyst (b) and Pd/MPC nanocatalyst (c).

In the catalyzed reduction reaction, the concentration of $NaBH_4$ was very high and could be considered as a constant during the reaction period; therefore, the rate constant for the reduction of 4-NP followed first-order kinetics.[44, 45] Plot of $\ln(C_t/C_0)$ versus time is obtained based on the absorbance as the function of time, and good linear correlations are observed, as shown in the reduction reaction catalyzed by Au/MPC (Fig. 7a) and Pd/MPC (Fig. 7b), indicating that the reactions follow first-order kinetics. The reaction rate constant k was calculated to be 1×10^{-2} s^{-1} and 1.2×10^{-2} s^{-1} for the reaction catalyzed using Au/MPC and Pd/MPC nanocatalyst, respectively. For a quantitative comparison, the activity parameter $k' = k/C_M$ was introduced, which is defined as the ratio of the rate constant k to the concentration of the active sites (Au or Pd) added. Thus, the k' was calculated to be $k_{Au}' = 2.54$ L s^{-1} g^{-1} and $k_{Pd}' = 23.48$ L s^{-1} g^{-1} for Au/MPC and Pd/MPC nanocatalyst, respectively. Obviously, Pd/MPC exhibited higher catalytic activity than Au/MPC. The values of activity parameter k' reported for Au NPs based catalysts, namely, Au/graphene

1   catalyst was 0.396 L s^{-1} g^{-1}.[46] However, the Pd NPs based catalyst Pd/PPy has the

2   activity parameter k$^{'}$ of about 2.94 L s^{-1} g^{-1}.[47] Thus, it could be concluded that the

3   synthesized nanocatalysts, Au/MPC and Pd/MPC, exhibited comparable or much

4   better catalytic activity than the reported catalysts for 4-NP reduction owing to their

5   higher catalytic performance, better selectivity, and longer stability.
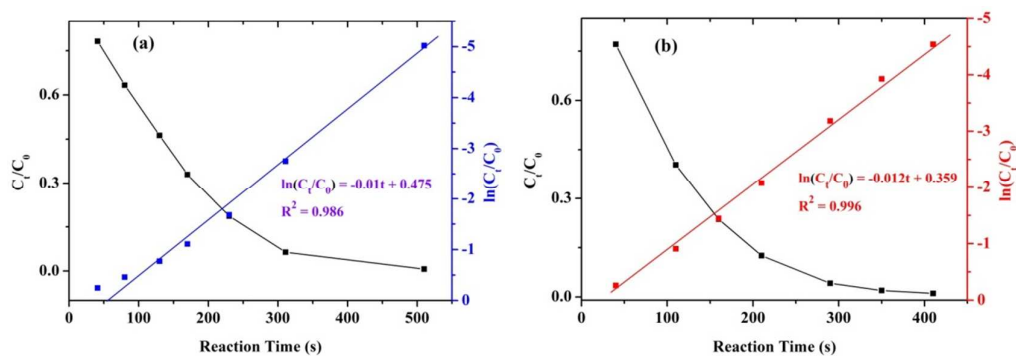
6
7   **Fig. 7.** Plots of C_t/C_0 and $\ln(C_t/C_0)$ versus reaction time for the reduction of 4-NP over Au/MPC nanocatalyst (a)
8   and Pd/MPC nanocatalyst (b).

9
10

11   ***HDC of 4-CP***

12   **Table 2.** Effect of different solvents and different bases.

13
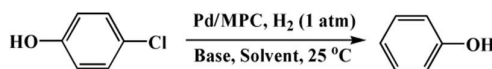
Entry	Base	Solvent	Yield
1	NaOH	C_2H_5OH	5%
2	NaOH	$CH_3COOC_2H_5$	22.7%
3	NaOH	DMF	14.7%
4	NaOH	H_2O	99.9%
5	Na_2CO_3	H_2O	78.7%
6	CH_3COONa	H_2O	93.4%
7	$NH_3 \cdot H_2O$	H_2O	58.9%
8	$(C_2H_5)_3N$	H_2O	68%

Conditions: 4-CP (0.5 mmol, 64.3 mg), base (0.5 mmol), solvent (30
mL), Pd/MPC (10 mg), H_2 balloon (30 mL/min), 25 °C, 2 h.

14

15   The abovementioned results clearly indicated that the Au/MPC and Pd/MPC

16   nanocatalysts exhibited the favorable catalytic performance toward reduction of 4-NP.

17   Their catalytic property and recyclability were also evaluated by performing HDC of

14

1   4-CP. Pd/MPC was used as a probe catalyst to optimize the reaction conditions and to

2   screen the best reaction conditions; therefore, a series of reactions was performed

3   using several bases and solvents to obtain the best possible combination (Table 2). In

4   order to prevent the poisoning of the catalysts, hydrochloric acid (HCl) produced

5   during the HDC process was neutralized by the bases added to the reaction system.[48]

6   Therefore, NaOH was first used as neutralizer to test different solvents (Table 2,

7   Entries 1–4). The yields of phenol in C_2H_5OH, $CH_3COOC_2H_5$, DMF, and H_2O were 5,

8   22.7, 14.7, and 99.9%, respectively. These low yields of phenol obtained in the

9   abovementioned organic solvents were mainly attributed to the low solubility property

10   of NaOH that leads to the poisoning of the nanocatalyst. Therefore, based on the

11   above mentioned results, H_2O was considered to be the best solvent for the HDC of

12   4-CP. To further optimize the reaction conditions; different bases were tested in the

13   aqueous solution (Table 2, Entries 4−8). The results indicated that the yield of the

14   phenol in the HDC reaction was significantly affected by the basicity of neutralizer

15   for HCl as reported by Zahara M. de Pedro.[49] The highest reaction rate and phenol

16   yield were achieved when the process was carried out in strong base (NaOH) solution.

17   In contrast, when a weak base was employed (Na_2CO_3, CH_3COONa, $NH_3 \cdot H_2O$, or

18   $(C_2H_5)_3N$), low yield of phenol was obtained under the same reaction conditions.

19   Therefore, NaOH was considered as the optimized base for HDC reaction.

20
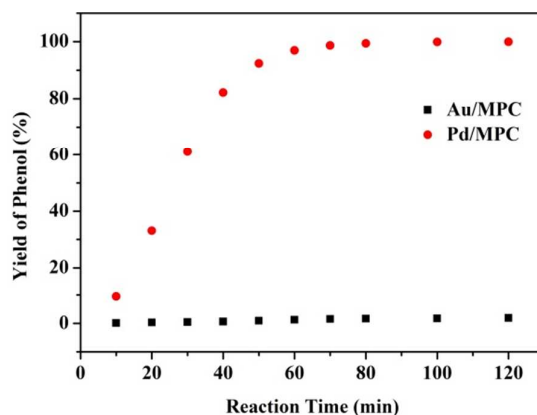
21

22   **Fig. 8.** Time evolution of the yield of phenol with Au/MPC and Pd/MPC nanocatalysts.

23

15

1 Thus, the catalytic property of Au/MPC and Pd/MPC in the HDC of 4-CP was

2 investigated using NaOH and H_2O as the optimized base and solvent, respectively. Fig.

3 8 shows that the time-dependent yield of phenol increases gradually, and reaches

4 almost 100% in 2 h when catalyzed by Pd/MPC composite under the optimized

5 reaction conditions, indicating that the Pd/MPC was highly active in HDC of 4-CP.

6 However, negligible amount of phenol was generated when the reaction was catalyzed

7 by Au/MPC, indicating that Au/MPC was almost inert toward the HDC of 4-CP. The

8 reason was that the catalyst support mesoporous carbon was non-reducible, thus, like

9 other non-reducible material (Al_2O_3 or SiO_2) supported Au catalysts, Au/MPC was

10 almost inert toward the hydrogen-mediated reactions.[50-52] However, Au supported on

11 the reducible support TiO_2 and Fe_3O_4 has been achieved superior catalytic response in

12 nitroaromatic and acetylene hydrogenation, respectively.[53, 54]

13 The reaction pathway of HDC of 4-CP over Pd/MPC was described as follows: First,

14 hydrogen was allowed to adsorb on the surface of the Pd NPs which dissociated into

15 two active hydrogen atoms; subsequently, the C–Cl bond of the adsorbed 4-CP was

16 attacked by the active hydrogen atoms to afford HCl and phenol. Simultaneously, HCl

17 was neutralized rapidly by NaOH; thus, avoiding the accumulation of HCl on the

18 surface of the catalyst.[55]
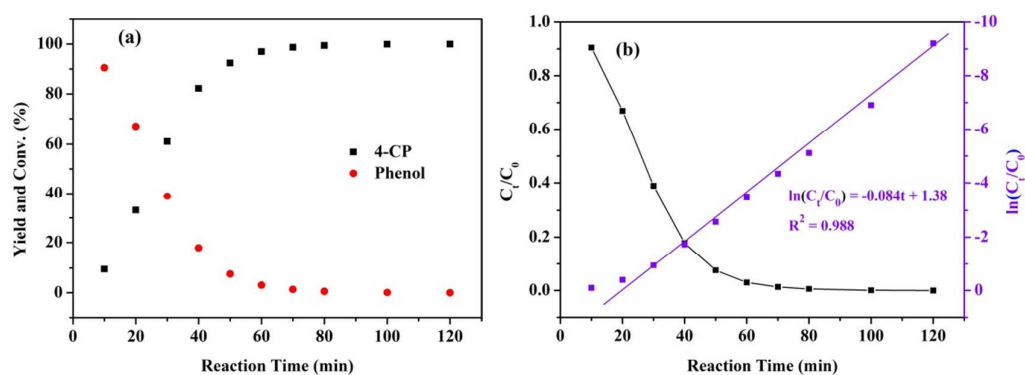
20 **Fig. 9.** (a) Time evolution of the yield of phenol and conversion of 4-CP with Pd/MPC nanocatalyst, (b) plots of

21 C_t/C_0 and $ln(C_t/C_0)$ versus reaction time for the HDC of 4-CP over Pd/MPC nanocatalyst.

23 The time evolution curves corresponding to the yield of phenol and conversion of

24 4-CP using Pd/MPC nanocatalyst are shown in Fig. 9a. H_2 was in the excessive

25 amount compared to 4-CP because it was bubbled into the reaction mixture; therefore,

1   it was considered as constant during the reaction period, thus the HDC reaction was

2   assumed to be pseudo first-order.[56] Therefore, by using the reaction kinetic $\ln(C_t/C_0) =$

3    $-kt$, the reaction rate constant k was calculated to be 0.084 min^{-1} for the reactions

4   catalyzed at room temperature with Pd/MPC nanocatalyst (Fig. 9b). The activity

5   parameter k' which is defined as the ratio of the rate constant k to the concentration of

6   the active sites was calculated to be 4.93 L g^{-1} min^{-1}. Compared to the reported Pd

7   NPs based catalytic systems PdAl-IMP-1.5 (2.33 L g^{-1} min^{-1}),[57] and Ni@Pd/KCC-1

8   (1.88 L g^{-1} min^{-1}),[58] obviously, the Pd/MPC nanocatalyst exhibited higher catalytic

9   activity, which was mainly attributed to the highly dispersed Pd NPs in the pores of

10   the MPC that enhanced the accessibility between the Pd active sites and 4-CP. Thus,

11   easy accessibility of the active sites favored the high catalytic activity.

12
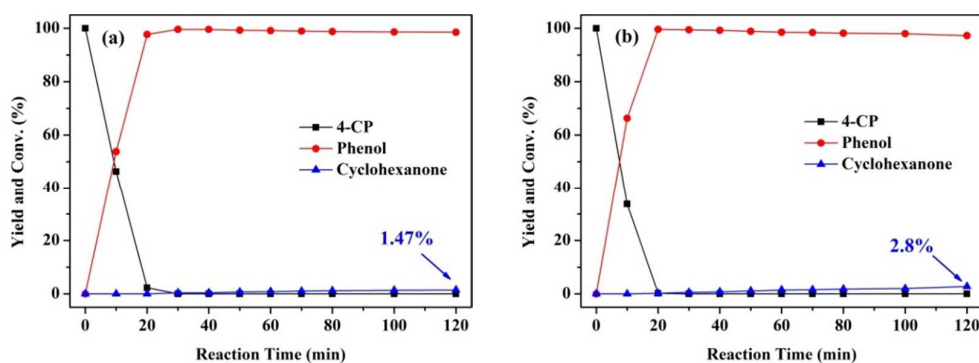
14   **Fig. 10.** Time evolution of the conversion of 4-CP and yield of phenol and cyclohexanone with 50 mg (a) and 100

15   mg (b) Pd/MPC nanocatalyst.

16   **Table 3.** Catalytic HDC of different substrates over Pd/MPC nanocatalyst

Entry	Reactants	Main products	Yield
1			99.8%
2			99.9%
3[a]			96.8%
4[b]			99.9%

Conditions: Chlorophenol (0.5 mmol), base (1 equiv.), solvent
(30 mL), Pd/MPC (10 mg), H_2 (30 mL/min), 25 °C, 2 h.
[a] 1 equiv. of NaOH,   [b] 2 equiv. of NaOH.

17

1   Under the optimized reaction conditions using Pd/MPC nanocatalyst (10 mg), the

2   HDC of 4-CP was completed in 2 h, and phenol was the only product detected by the

3   GC–MS. When the catalyst dosage is increased to 50 and 100 mg, the HDC of 4-CP is

4   completed in 30 (Fig. 10a) and 20 min (Fig. 10b), respectively. When the reaction is

5   continued for 2 h, 1.47% and 2.8% of cyclohexanone are generated along with phenol

6   (Fig. 10). This was attributed to the high concentration of catalyst that showed activity

7   for hydrogenation of phenol to form cyclohexanone as the byproduct. This

8   phenomenon has also been reported in the literatures.[56, 59, 60] Effect of dosage of 4-CP

9   on the HDC of 4-CP catalyzed by 10 mg of Pd/MPC was also studied, and the results

10   are illustrated in Fig. S2a. A decrease in yield of phenol was observed with increasing

11   dosage of 4-CP. The HDC reaction could be completed in 2 h under the optimized

12   reaction conditions with 10 mg Pd/MPC nanocatalyst and 0.5 mmol of 4-CP. However,

13   when 2 and 8 mmol of 4-CP were introduced, the yields of phenol were only 81 and

14   64.4% in 2 h, respectively (Fig. S2a). Effect of Pd loading of the Pd/MPC for the

15   HDC of 4-CP was further investigated. As shown in Fig. S2b, with higher Pd loading

16   (7.83%), the Pd/MPC catalyzed HDC of 4-CP could be completed in 1 h. While with

17   lower Pd loading (2.56%), in the same reaction conditions, the HDC reaction could

18   not be completed in 2 h, the yield of phenol was about 97%.

19   In order to investigate the application of the Pd/MPC nanocatalyst for HDC of

20   chlorophenols, we also studied the HDC of 2-CP, 3-CP and 2,4-dichlorophenol (2,

21   4-DCP) catalyzed by Pd/MPC nanocatalyst and the corresponding results are listed in

22   Table 3. The values listed in Table 3 reveal that, 3-CP and 2-CP are also almost

23   completely transformed into phenol within 2 h. However, for 2, 4-DCP, when just 1

24   equivalent of NaOH was introduced, the main product was 2-CP; further, it was

25   completely transformed into phenol when 2 equivalents of NaOH were added into the

26   reaction mixture. Thus, 2-CP was the only intermediate product identified in the HDC

27   of 2, 4-DCP reaction system as described in the previous work.[61] The completely

28   HDC of 2, 4-DCP was accomplished by two steps.[50] The reason was ascribed

29   probably to the electronic and steric hindrance of 2, 4-DCP.
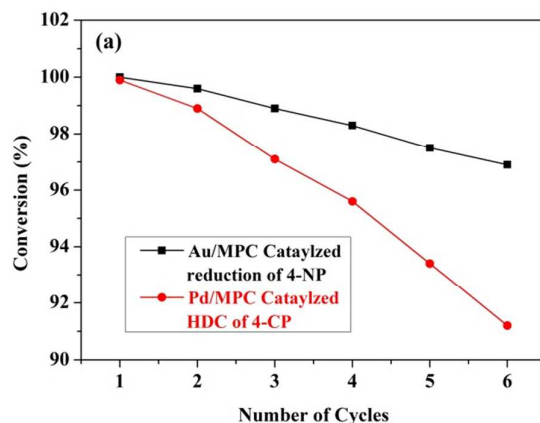
1

2   **Fig. 11.** The reusability of Au/MPC for the reduction of 4-NP with NaBH$_4$ and Pd/MPC for the HDC of 4-CP.

3

4   Moreover, the advantage of the Au/MPC and Pd/MPC nanocatalysts prepared in this

5   study was that the catalysts were conveniently recovered by magnetic separation. It is

6   well known that magnetic separation is an appealing alternative for filtration or

7   centrifugation as it prevents the loss of catalyst and improves its reusability for the

8   liquid-phase reactions.[62] The recovery and reusability of Au/MPC and Pd/MPC were

9   investigated by the reduction of 4-NP and HDC of 4-CP, respectively. Fig. 11 shows

10   that the Au/MPC nanocatalyst could be successfully recycled and reused for at least

11   six times with a stable conversion above 96% within 10 min in the reduction of 4-NP.

12   However, in the HDC of 4-CP, there was a slight decrease in the conversion of 4-CP

13   with the increase in the number of runs, probably due to the gradual leaching of Pd

14   NPs with repeated magnetic separation and poisoning of Pd NPs active centers via

15   oxidation or catalyst inactivation. The ICP–AES analysis also showed that after six

16   catalytic runs there were about 3.76 wt% of Au and 4.92 wt% of Pd in Au/MPC and

17   Pd/MPC nanocatalysts, respectively, indicating slight leaching of the noble metals.

18   However, the TEM revealed that the morphologies of the Au/MPC and Pd/MPC

19   nanocatalysts were still maintained even after six catalytic cycles (Fig. S3a and b).

20   The EDX mapping indicated that the Au and Pd NPs were still dispersed on the MPC

21   support (Fig. S3c and d). Additionally, the EDS spectra of Au/MPC and Pd/MPC

22   nanocatalysts also confirmed that the chemical composition did not change after six

23   cycles (Fig. S3e and f).

1 **Conclusions**

2 This study demonstrated that the immobilization of Au and Pd NPs within the pores of

3 the mesoporous MPC efficiently enhanced the catalytic activities, separation, and

4 reusability of the Au/MPC and Pd/MPC nanocatalysts. Both the Au/MPC and

5 Pd/MPC nanocatalysts exhibited comparable or better catalytic activity than most of

6 the reported catalysts used for the reduction of 4-NP. Moreover, the Pd/MPC

7 nanocatalyst displayed high efficiency in the HDC of chlorophenols. Further, the

8 MPC based nanocatalysts could be easily recovered from the reaction mixture by

9 using a magnet and reused for the next catalytic run. These methods represent an

10 eco-friendly strategy to dispose nitro- and chloro- compounds. This study provides a

11 general methodology for the preparation of other NMNPs/MPC nanocomposites with

12 high catalytic activity and good magnetic recycling properties for various industrial

13 catalytic applications.

14 **Acknowledgements**

18 **References**

19 1.   S.-i. Yamamoto, H. Kinoshita, H. Hashimoto and Y. Nishina, *Nanoscale*, 2014,

20   6, 6501-6505.

21 2.   F. Gonzalez de Rivera, I. Angurell, M. D. Rossell, R. Erni, J. Llorca, N. J.

22   Divins, G. Muller, M. Seco and O. Rossell, *Chem. Eur. J.*, 2013, 19,

23   11963-11974.

24 3.   X. Yang, D. Chen, S. J. Liao, H. Y. Song, Y. W. Li, Z. Y. Fu and Y. L. Su, *J.

25   Catal.*, 2012, 291, 36-43.

26 4.   D. Shuai, D. C. McCalman, J. K. Choe, J. R. Shapley, W. F. Schneider and C. J.

27   Werth, *ACS Catal.*, 2013, 3, 453-463.

28 5.   L. Yuwen, F. Xu, B. Xue, Z. Luo, Q. Zhang, B. Bao, S. Su, L. Weng, W.

Huang and L. Wang, *Nanoscale*, 2014, 6, 5762-5769.

6.   H. Mao, S. Peng, H. Yu, J. Chen, S. Zhao and F. Huo, *J. Mater. Chem. A*, 2014, 2, 5847-5851.

7.   M. Chu, Y. Zhang, L. Yang, Y. Tan, W. Deng, M. Ma, X. Su, Q. Xie and S. Yao, *Energ. Environ. Sci.*, 2013, 6, 3600-3604.

8.   C. Ma, W. Xue, J. Li, W. Xing and Z. Hao, *Green. Chem.*, 2013, 15, 1035-1041.

9.   Y. Lin, Y. Qiao, Y. Wang, Y. Yan and J. Huang, *J. Mater. Chem.*, 2012, 22, 18314-18320.

10.   M. Zhao, K. Deng, L. He, Y. Liu, G. Li, H. Zhao and Z. Tang, *J. Am. Chem. Soc.*, 2014, 136, 1738-1741.

11.   Y. Chen, H.-R. Chen and J.-L. Shi, *Acc. Chem. Res.*, 2014, 47, 125-137.

12.   B. Xia, Y. Yan, X. Wang and X. W. Lou, *Materials Horizons*, 2014, 1, 379-399.

13.   Y. Yan, B. Xia, Z. Xu and X. Wang, *ACS Catal.*, 2014, 4, 1693-1705.

14.   J. Lee, O. K. Farha, J. Roberts, K. A. Scheidt, S. T. Nguyen and J. T. Hupp, *Chem. Soc. Rev.*, 2009, 38, 1450-1459.

15.   G. Ozkan, S. Gok and G. Ozkan, *Chem. Eng. J.*, 2011, 171, 1270-1275.

16.   X. Wan, C. Zhou, J. Chen, W. Deng, Q. Zhang, Y. Yang and Y. Wang, *ACS Catal.*, 2014, 4, 2175-2185.

17.   H. Li, L. Han, J. Cooper-White and I. Kim, *Green. Chem.*, 2012, 14, 586-591.

18.   H. Joshi, K. N. Sharma, A. K. Sharma and A. K. Singh, *Nanoscale*, 2014, 6, 4588-4597.

19.   R. Wang, Z. Wu, C. Chen, Z. Qin, H. Zhu, G. Wang, H. Wang, C. Wu, W. Dong, W. Fan and J. Wang, *Chem. Commun.*, 2013, 49, 8250-8252.

20.   J. Liu, X. Huo, T. Li, Z. Yang, P. Xi, Z. Wang and B. Wang, *Chem. Eur. J.*, 2014, 20, 11549-11555.

21.   L. Zhang, Z. Su, F. Jiang, L. Yang, J. Qian, Y. Zhou, W. Li and M. Hong, *Nanoscale*, 2014, 6, 6590-6602.

22.   X. Yan, X. Li, Z. Yan and S. Komarneni, *Appl. Surf. Sci.*, 2014, 308, 306-310.

23. W. Cho, S. Park and M. Oh, *Chem. Commun.*, 2011, 47, 4138-4140.

24. H. J. Lee, W. Cho, E. Lim and M. Oh, *Chem. Commun.*, 2014, 50, 5476-5479.

25. N. Li, M. Echeverria, S. Moya, J. Ruiz and D. Astruc, *Inorg. Chem.*, 2014, 53, 6954-6961.

26. M. Muniz-Miranda, *Appl. Catal. B: Environ.*, 2014, 146, 147-150.

27. Z. Sun, X. Wei, Y. Han, S. Tong and X. Hu, *J. Hazard. Mater.*, 2013, 244, 287-294.

28. J. A. Baeza, L. Calvo, M. A. Gilarranz and J. J. Rodriguez, *Chem. Eng. J.*, 2014, 240, 271-280.

29. S. M. El-Sheikh, A. A. Ismail and J. F. Al-Sharab, *New J. Chem.*, 2013, 37, 2399-2407.

30. C. Serre, F. Millange, S. Surblé and G. Férey, *Angew. Chem. Int. Edit.*, 2004, 43, 6285-6289.

31. S. Yan and S. Zhang, *Int. J. Hydrogen. Energ.*, 2011, 36, 13392-13397.

32. S. Yan, L. Gao, S. Zhang, W. Zhang, Y. Li and L. Gao, *Electrochimica Acta*, 2013, 94, 159-164.

33. M. Turáková, M. Králik, P. Lehocký, Ľ. Pikna, M. Smrčová, D. Remeteiová and A. Hudák, *Appl. Catal. A: General*, 2014, 476, 103-112.

34. B. Duan, F. Liu, M. He and L. Zhang, *Green. Chem.*, 2014, 16, 2835-2845.

35. S. Dutta, S. Sarkar, C. Ray, A. Roy, R. Sahoo and T. Pal, *ACS Appl. Mater. Interf.*, 2014, 6, 9134-9143.

36. X. Chen, Z. Cai, X. Chen and M. Oyama, *J. Mater. Chem. A*, 2014, 2, 5668-5674.

37. S. P. Prakash and K. R. Gopidas, *Chemcatchem*, 2014, 6, 1641-1651.

38. Y. Xia, T. Li, C. Ma, C. Gao and J. Chen, *Rsc Adv.*, 2014, 4, 20516-20520.

39. H. Li, S. Gan, D. Han, W. Ma, B. Cai, W. Zhang, Q. Zhang and L. Niu, *J. Mater. Chem. A*, 2014, 2, 3461-3467.

40. Y.-Y. Shen, Y. Sun, L.-N. Zhou, Y.-J. Li and E. S. Yeung, *J. Mater. Chem. A*, 2014, 2, 2977-2984.

41. B. Liu, S. Yu, Q. Wang, W. Hu, P. Jing, Y. Liu, W. Jia, Y. Liu, L. Liu and J.

Zhang, *Chem. Commun.*, 2013, 49, 3757-3759.

42.   Q. Wang, W. Jia, B. Liu, A. Dong, X. Gong, C. Li, P. Jing, Y. Li, G. Xu and J. Zhang, *J. Mater. Chem. A*, 2013, 1, 12732-12741.

43.   J. Zheng, Y. Dong, W. Wang, Y. Ma, J. Hu, X. Chen and X. Chen, *Nanoscale*, 2013, 5, 4894-4901.

44.   X. Gu, W. Qi, X. Xu, Z. Sun, L. Zhang, W. Liu, X. Pan and D. Su, *Nanoscale*, 2014, 6, 6609-6616.

45.   K. Dong, Z. Liu and J. S. Ren, *Crystengcomm*, 2013, 15, 6329-6334.

46.   J. Li, C. Y. Liu and Y. Liu, *J. Mater. Chem.*, 2012, 22, 8426-8430.

47.   Y. Xue, X. Lu, X. Bian, J. Lei and C. Wang, *J. Coll. Interf. Sci.*, 2012, 379, 89-93.

48.   C. Sun, Z. Wu, Y. Mao, X. Yin, L. Ma, D. Wang and M. Zhang, *Catal. Lett.*, 2011, 141, 792-798.

49.   Z. M. de Pedro, E. Diaz, A. F. Mohedano, J. A. Casas and J. J. Rodriguez, *Appl. Catal. B: Environ.*, 2011, 103, 128-135.

50.   S. Gomez-Quero, F. Cardenas-Lizana and M. A. Keane, *J. Catal.*, 2013, 303, 41-49.

51.   F. Cárdenas-Lizana, S. Gómez-Quero and M. A. Keane, *ChemSusChem*, 2008, 1, 215-221.

52.   A. C. Gluhoi, M. A. P. Dekkers and B. E. Nieuwenhuys, *J. Catal.*, 2003, 219, 197-205.

53.   A.Sárkány, Z. Schay, K. Frey, É. Széles and I. Sajó, *Appl. Catal. A: General*, 2010, 380, 133-141.

54.   M. Boronat, P. Concepción, A. Corma, S. González, F. Illas and P. Serna, *J. Am. Chem. Soc.*, 2007, 129, 16230-16237.

55.   S. Wang, B. Yang, T. Zhang, G. Yu, S. Deng and J. Huang, *Ind. Eng. Chem. Res.*, 2010, 49, 4561-4565.

56.   E. Diaz, J. A. Casas, A. F. Mohedano, L. Calvo, M. A. Gilarranz and J. J. Rodriguez, *Ind. Eng. Chem. Res.*, 2008, 47, 3840-3846.

57.   C. B. Molina, L. Calvo, M. A. Gilarranz, J. A. Casas and J. J. Rodriguez, *J.

1   *Hazard. Mater.*, 2009, 172, 214-223.

2   58.   Z. Dong, X. Le, C. Dong, W. Zhang, X. Li and J. Ma, *Appl. Catal. B: Environ.*,

3   2015, 162, 372-380.

4   59.   J. A. Baeza, L. Calvo, M. A. Gilarranz, A. F. Mohedano, J. A. Casas and J. J.

5   Rodriguez, *J. Catal.*, 2012, 293, 85-93.

6   60.   M. Munoz, Z. M. de Pedro, J. A. Casas and J. J. Rodriguez, *Water Res.*, 2013,

7   47, 3070-3080.

8   61.   J. Zhou, K. Wu, W. Wang, Z. Xu, H. Wan and S. Zheng, *Appl. Catal. A:*

9   *General*, 2014, 470, 336-343.

10   62.   F. Zhang, J. Jin, X. Zhong, S. Li, J. Niu, R. Li and J. Ma, *Green. Chem.*, 2011,

11   13, 1238-1243.

12

Graphical Abstract

The magnetic porous carbon composite which has been synthesized from metal organic framework is used as catalysts support to fabricate Au and Pd NPs based nanocatalysts.